Marine Biotechnology (2022) 24:203–215
https://doi.org/10.1007/s10126-022-10099-y

ORIGINAL ARTICLE

Structural Characterization and Immunoenhancing Effects of a Polysaccharide from the Soft Coral *Lobophytum sarcophytoides*

Xueqin Cao[1] · Qian Zhang[1] · Yanglu Zhu[1] · Siju Li[1] · Ying Cai[1] · Pei Li[2] · Deliang Liu[1] · Yun Leng[1] · Simin Ye[1] · Zengmei Xu[1] · Hao Li[1] · Baochun Shen[3] · Qiongfeng Liao[2] · Lan Liu[4] · Zhiyong Xie[1]

Received: 13 October 2021 / Accepted: 21 January 2022 / Published online: 17 February 2022

Abstract

Previous studies on the soft coral *Lobophytum sarcophytoides* (*Lobophytum* sp.) are mainly about small molecules, and there has been no systematic research on polysaccharides. In the study, a novel polysaccharide (LCPs-1-A) with immunoenhancing functions was successfully extracted and purified from the soft coral *Lobophytum* sp. After preliminary analysis, our data indicated that LCPs-1-A was composed of glucose and had a molecular weight of 4.90×10^6 Da. Moreover, our findings showed that LCPs-1-A could promote the proliferation and phagocytosis of RAW264.7 cells, stimulate the production of NO and ROS, and increase the mRNA expression of IL-1β, IL-6, and TNF-α, which indicated that LCPs-1-A had a good immunoenhancing activity. Through further studies, we found that LCPs-1-A might play an immunoenhancing role through the TLR4/NF-κB signaling pathway. Therefore, our results demonstrated that LCPs-1-A might be a natural immunostimulant for use in medical and food industries.

Keywords Polysaccharide · Soft coral *Lobophytum sarcophytoides* · RAW264.7 cell · Immunostimulant · TLR4/NF-κB signaling pathway · Structural characterization

Introduction

The ocean occupies 70% of the Earth's surface, equivalent to 90% of the biosphere (Ruocco et al. 2016), so marine life is a rich source for the discovery of new natural compounds. Due to the particularity of the oceanic environment, the structures and activities of the polysaccharides produced by marine organisms are different from those generated by land organisms (Simmons et al. 2005; Molinski et al. 2009). Polysaccharides from marine sources have many biological activities, such as antioxidant (Liu et al. 2012), immunoregulatory (Safari and Hassan 2020), anticoagulant (Synytsya et al. 2015), antitumor (da Silva Barbosa et al. 2021), hypoglycemic (Zhu et al. 2020), and lipid-lowering effects (Liu et al. 2012). There are also many polysaccharides from ocean organisms that have been applied in daily life, such as chitin extracted from shellfish, shrimp, and crab shells, which are widely used in medicine and the biomedical field (Younes and Rinaudo 2015). The soft coral *Lobophytum* sp. is a marine lower invertebrate that is common in tropical and subtropical seas. It is known that the main areas of research on the soft coral are terpenoids, steroids, and other small molecule substances (Shen et al. 2019; Ye et al. 2020), and studies on polysaccharides have not yet been reported.

Macrophages are important in the innate immune system, can kill pathogens directly by phagocytosis, and can produce toxic effects by secreting IL-1β, IL-6, TNF-α, NO, ROS, etc. (Schepetkin and Quinn 2006). Polysaccharides are high-molecular-mass polymers that can bind to pattern recognition receptors (PRRs) on cell membranes to form heterodimers and then recruit different adapters to regulate downstream gene expression (Takeuchi and Akira 2010; Couto and Zipfel 2016). It has been reported that most

✉ Zhiyong Xie
xiezhy@mail.sysu.edu.cn

1 School of Pharmaceutical Sciences (Shenzhen), Sun Yat-Sen University, 132 Waihuan East Road, Guangzhou 510006, People's Republic of China

2 School of Pharmaceutical Sciences, Guangzhou University of Chinese Medicine, Guangzhou 510006, People's Republic of China

3 School of Pharmacy, Kunming Medical University, Kunming 650500, People's Republic of China

4 School of Marine Sciences, Sun Yat-Sen University, Guangzhou 510006, People's Republic of China

polysaccharides can enter macrophages through PRRs on the cytomembrane and exert immunoenhancing effects (Yan et al. 2018). In this study, LCPs-1-A, with immunoenhancing functions, was isolated from soft coral, and its structure was preliminarily characterized.

Materials and Methods

Materials and Reagents

The soft coral *Lobophytum* sp. was sampled at 112° 44′ 53.37″ E, 16° 40′ 11.88″ N, 23 m underwater, east of Xisha Island in July 2018. This soft coral was provided and identified by Lan Liu, a professor at the School of Marine Sciences at Sun Yat-sen University.

RAW264.7 cells were obtained from the Institute of Cell Biology, Chinese Academy Sciences (Shanghai, China), and reagents used for cell culture were ordered from Gibco Life Technologies (Grand Island, NY, USA). DEAE-cellulose-52 (DEAE-52), methylthiazolyldiphenyl-tetrazolium bromide (MTT), polymyxin B, neutral red, and Triton X-100 were purchased from Beijing Soledad Science and Technology Co., Ltd. (Beijing, China), and Sephacryl 300 HR was purchased from Shanghai Yuanye Bio-Technology Co. Ltd (Shanghai, China). The dextran standards, monosaccharide standards, lipopolysaccharide (LPS), 1-phenyl-3-methyl-5-pyrazolone (PMP), and trifluoroacetic acid (TFA) were ordered from Sigma-Aldrich (MO, USA). NO assay kits, ROS assay kits, and 4′,6-diamidino-2-phenylindole (DAPI) were purchased from Beyotime Biotechnology Co. Ltd (Beijing, China). TRIzol reagent was purchased from Ambion (Austin, TX, USA), and primer synthesis was commissioned by Sangon Biotech Co. Ltd. (Shanghai, China). The BCA protein assay kit was purchased from Beijing Cowin Biotech Co. Ltd. (Beijing, China). Enhanced chemiluminescence (ECL) kits were purchased from FdBio Science Biotech Co. Ltd. (Hangzhou, China). Primary antibodies were purchased from Abcam, FdBio Science Biotech Co. Ltd. (Hangzhou, China) and Affinity Biosciences Ltd. (USA). Deionized water was purified using a Milli-Q system (Milford, MA, USA). The other chemicals were of analytical grade and were provided by Damao Chemical Regent Factory (Tianjin, China).

Preparation of the Crude Polysaccharide

Extraction of the crude polysaccharides was based on a reported method (Lee et al. 2011). Soxhlet extraction was carried out with petroleum ether to remove lipophilic components and pigments from coral powder. After siphoning at 85 °C for 3 h, the treated powder was placed in an oven at 60 °C to dry overnight. The dried powder was mixed with water at a ratio of 10 mL/g, and extracted twice at 100 °C for 4 h. Then, the filtrate was concentrated with a rotary evaporator, and 4 times the volume of 95% ethanol was added under stirring. After standing at 4 °C for 12 h, the precipitated crude polysaccharide could be obtained by centrifuging at 5000 rpm for 20 min and was named as LCPs.

Separation and Purification of LCPs

Crude polysaccharides contain proteins, which can be removed by protease and the Sevag method (Song et al. 2017). The crude polysaccharide was redissolved in deionized water, and papain was added (1 mg/mL). The reaction solution was stirred continuously at 60 °C for 4 h. After the reaction, the solution was heated at 100 °C for 15 min, cooled to room temperature, and centrifuged at 5000 rpm for 20 min. The Sevag reagent (chloroform:n-butanol = 4:1, V/V) was added to the clear supernatant at a volume ratio of 10:1 (supernatant: Sevag reagent = 10:1, V/V), followed by vortexing for 5 min and centrifugation at 5000 rpm for 15 min. The supernatant obtained by centrifugation underwent repeated iterations of the Sevag method until the proteins were removed. The final solution was dried with a rotary evaporator to remove the chemical reagents, redissolved in deionized water, and dialyzed for 24 h, changing the water every 3 h. Finally, the samples were lyophilized to obtain crude polysaccharides without proteins.

Crude polysaccharides without proteins (0.4 g) were dissolved in 5 mL of distilled water and filtered. The solution was separated by a DEAE-52 column (2.6 × 30 cm) and eluted with NaCl solutions at different concentrations (Chu et al. 2019). The sampling speed was 0.8 mL/min (10 min/tube) and the solutions in the tubes were analyzed by the phenol–sulfuric acid method (Dubois et al. 1956). Then, the products were collected, concentrated, dialyzed, and lyophilized. LCPs-1 (60 mg) with the highest purity was dissolved in 5 mL of distilled water and filtered. The samples were separated on a Sephacryl 300 HR dextran gel column (1.6 × 90 cm) and eluted with 0.1 M NaCl solution at a flow rate of 0.5 mL/min (10 min/tube) for further purification (Song et al. 2017). In the same way, the purified polysaccharide was collected and designated LCPs-1-A.

Characterization of LCPs-1-A

LCPs-1-A was dissolved in deionized water, and the UV spectrum of LCPs-1-A at 190 ~ 400 nm was determined with a UV–Vis spectrophotometer (UV-2600, Shimadzu, Japan) (Liu et al. 2016).

LCPs-1-A (1 mg/mL) was filtered through a 0.22-μm filter membrane. The molecular weight of the sample was determined by HPGPC (Gao et al. 2009), which was performed with an LC-20A HPLC system (Shimadzu, Tokyo,

Japan) equipped with a PolySEP-GFC-P 4000 column (Phenomenex, 300 × 7.8 mm) and an evaporative light scattering detector (ELSD). The temperature of the detector was set at 60 °C, the gain value was 10, and the column temperature was 35 °C. Ultra-pure water was used as the mobile phase, and the flow rate was 1.0 mL/min. The injection volume was 20 µL. A standard curve of molecular weight was constructed with dextran standards at the same concentration.

LCPs-1-A was scanned in the range of 4000 ~ 400 cm^{-1} with a Fourier transform infrared spectrometer (Spectrum Two, PerkinElmer, USA), and the data were recorded (Wang et al. 2017).

The monosaccharide composition was analyzed according to a previously reported method with some modifications (Lin et al. 2020). Briefly, LCPs-1-A (5 mg) was hydrolyzed with 2 mL of 3 MTFA at 120 °C for 6 h. After that, 1 ~ 2 mL of methanol was added to the reaction solution, and the solution was dried with a rotary evaporator; this process was repeated three times to remove excess TFA. The hydrolysate was redissolved in deionized water (800 µL), 0.3 M NaOH (100 µL), and a 0.5 M PMP methanol solution (100 µL), mixed and reacted at 70 °C for 30 min. After cooling, 0.3 M HCl (105 µL), deionized water (200 µL), and chloroform (700 µL) were added. Last, we removed PMP by centrifugation. The upper aqueous phase was filtered through a 0.22-µm membrane and analyzed with an HPLC system (LC-20A, Shimadzu) with a C18 column (4.6 × 250 mm i.d. 5 µm, Waters) and an ultraviolet detector. The flow rate was 1.0 mL/min with 0.1 M phosphate buffer (pH 6.7) -acetonitrile (83:17). The sample volume was 20 µL for detection. Meanwhile, the monosaccharide standards were subjected to the same treatments.

LCPs-1-A (30 mg) was dissolved in D_2O (0.55 ml) and lyophilized, and this process was repeated three times. Finally, D_2O (0.55 mL) was added to the sample, and a 600 MHz NMR apparatus (Bruker BioSpin, Germany) was used for structural determination (Liao et al. 2018). ^{1}H NMR and ^{13}C NMR spectra were recorded.

Determination of Immune Activity in RAW264.7 Cells

Cell Culture

RAW264.7 cells were derived from BALB/c mouse mononuclear macrophages, which is a classical cell model for studying the immune response in vitro. RAW264.7 cells were cultured at 37 °C in DMEM (Gibco, USA) supplemented with 10% fetal bovine serum (Gibco, USA) and 1% penicillin and streptomycin (Gibco, USA) in a 5% CO2 incubator (Wang et al. 2019).

Cell Viability Assay

The cell viability assay was based on a reported method (Mosmann 1983). RAW264.7 cells were inoculated into 96-well plates at a density of 2×10^4 cells/well for 12 h of adherent growth. The old culture medium was discarded, and new culture medium was added to the cells with 2, 4, 6, 8, 10, or 12 µg/ml LCPs-1-A. The control group and positive drug group were treated with culture medium and LPS (1 µg/mL), respectively, and the cells were incubated for 24 h. At the end of incubation, the cells were observed under a microscope. After the observation, the supernatant was discarded, and 20 µL of MTT (5 mg/mL) solution was added to each well. After 4 h, the supernatant was removed, and 200 µL of DMSO was added for cell lysis and crystal solubilization. Then, the absorbance at 490 nm was measured with a microplate reader after shaking on a horizontal shaker for 10 min.

Neutral Red Uptake Assay

The phagocytic ability was measured by a neutral red uptake assay (Weeks et al. 1987; Liu et al. 2017b). RAW264.7 cells (1×10^5 cells/well) were seeded into 96-well plates and incubated for 12 h. Different groups were treated with culture medium, LCPs-1-A or LPS for 24 h. After that, the supernatant was removed, and 100 µL of 0.75 mg/mL neutral red-PBS solution was added to each well and incubated for 45 min. Finally, the supernatant was discarded, the cells were washed with PBS three times, and then 100 µL/well cell lysis buffer (ethanol: glacial acetic acid = 1:1, V/V) was added. After 2 h, the absorbance was measured at 540 nm.

NO Production Determination

RAW264.7 cells (2×10^5 cells/well) were plated in 96-well plates and incubated overnight. The old medium was discarded, and the cells were treated with culture medium, LCPs-1-A or LPS. After 24 h of cultivation, 50 µL of the supernatant was taken, and the same volume of Griess reagent was added. The absorbance was measured at 540 nm with a microplate reader after the mixed solution incubated at 37 °C for 10 min. Additionally, $NaNO_2$ was used as a standard product to prepare the standard curve, and the concentration of NO in the supernatant of each group was determined with the standard curve (Yu et al. 2013).

Polymyxin B (PMB) is a specific antagonist of LPS (Velkov et al. 2013). To exclude the interference from endotoxin in LCPs-1-A, confirmatory experiments were conducted with or without the addition of PMB to the samples, which could determine whether endotoxin was contained in LCPS-1-A by detecting the expression level of NO.

Effect of LCPs-1-A on the Production of ROS

The fluorescence intensity of ROS was assessed by a reported method with some modifications (Rastogi et al. 2010; Sadhu et al. 2019). RAW264.7 cells (3×10^5 cells/dish) were seeded in confocal dishes overnight, then the medium was discarded, and the cells were treated with blank medium, LPS (1 μg/mL) or LCPs-1-A (12 μg/mL). Incubation was continued for 24 h. The cells were then washed with PBS and DMEM with 0.1% DCFH-DA was added followed by incubation for another 30 min. The cells were fixed with 4% paraformaldehyde in PBS for 30 min, washed with PBS again, and 0.2% Triton X-100 in PBS was added for 10 min, which was used to increase cell permeability. After washing with PBS, the cells were treated with DAPI for staining. After 15 min, the cells were washed and observed under a confocal microscope (LSM880, Zeiss, Germany) and all images were acquired using the same intensity and photodetector.

The determination of ROS was referred to the reported assay (Ren et al. 2017). RAW264.7 cells (1×10^5 cells/well) were inoculated into 96-well plates for 12 h. After treating with culture medium, LCPs-1-A or LPS for 24 h, the supernatant was removed, and DMEM with 0.1% DCFH-DA was added to cells after rinsing with PBS three times, followed by further incubation for 30 min in the dark. The cells were suspended in PBS after washing with PBS. The fluorescence intensity of cell suspension was measured at 500-nm excitation and 525-nm emission wavelengths using a fluorescence microplate reader (FilterMaxF5, Molecular Devices, USA).

Quantitative Real-Time PCR (qRT-PCR) Analysis

RAW264.7 cells (1×10^6 cells/well) were plated in 6-well plates for 12 h, and different concentrations of LCPs-1-A and LPS were added to stimulate the cells. After 24 h of culture, RNA was extracted with TRIzol reagent, reverse-transcribed into cDNA with a reverse transcription kit, and then amplified into cDNA. Real-time PCR was performed with the incorporation of SYBR green using a LightCycler 480 real-time PCR system (Roche). Program settings and primer sequences are shown in the Tables 1 and 2. Relative expression levels of the target genes were analyzed by the $2^{-\Delta\Delta Ct}$ method with GAPDH as an internal reference (Yuan et al. 2020).

Table 1 Amplification program of qRT-PCR

	Reaction temperature	Reaction time
Predegeneration	95 °C	30 s
PCR reaction	95 °C	5 s
(×40 cycles)	60 °C	10 s
	75 °C	15 s

Table 2 Primer sequences of real-time PCR analysis

Genes		Sequences (5′→3′)
GAPDH	Forward	GTGTTCCTACCCCCAATGTGT
	Reverse	ATTGTCATACCAGGAAATGAGCTT
IL-1β	Forward	CTTCAGGCAGGCAGTATCACTC
	Reverse	TGCAGTTGTCTAATGGGAACGT
IL-6	Forward	CCTACCCCAATTTCCAATGCTC
	Reverse	GGTCTTGGTCCTTAGCCACTC
TNF-α	Forward	GATCGGTCCCCAAAGGGATG
	Reverse	GTGGTTTGTGAGTGTGAGGGT

Immunofluorescence Assay for NF-κB

The nuclear translocation of NF-κB was evaluated by the immunofluorescence assay (Wu et al. 2020). RAW264.7 cells (5×10^5 cells/dish) were inoculated in confocal dishes. After overnight culture, the cells were treated with culture medium, LCPs-1-A or LPS for 24 h, fixed, and successively permeated. Then, 1% BSA in PBS was added to block the cells at room temperature for 1 h, and NF-κB p65 antibody in 1% BSA (1:200) was added for incubation overnight at 4 °C. After rinsing with PBS, the secondary antibody in 1% BSA (1:200) was added and incubated at 37 °C for 1 h. After washing, DAPI was added for staining for 15 min. After washing again, the cells were observed under a confocal microscope and all images were obtained using the same intensity and photodetector.

Western Blot Analysis

RAW264.7 cells (2 million cells/well) were seeded onto six-well plates for one night and then treated with culture medium, LCPs-1-A or LPS for 2 h. Protein was extracted on ice, and cells were lysed with cell lysis buffer (RIPA: PMSF = 50:1, V/V, plus one part phosphatase inhibitor per 10 mL). Next, the supernatant was collected and quantified with a BCA protein assay kit. Finally, the protein was denatured at 100 °C. The denatured protein (20 μg) was separated by 10% SDS–PAGE, and the bands were transferred to polyvinylidene fluoride membranes and then sealed with BSA blocking solution for 2 h. After cutting the membranes, diluted primary antibodies (Table 3) were added for incubation overnight. The membranes were washed with TBST three times, and diluted secondary antibodies (1:3000) were added and incubated for 2 h. The target bands were detected with ECL kits and recorded with a Chem Studio 815 system (UVP, USA). ImageJ was used to analyze the bands, with β-Tubulin as an internal reference (Jeong et al. 2019).

Table 3 Information of antibodies employed in western blot

Name	Cat. no. species	Dilution
TLR4	ab95562, Rat monoclonal IgG	1:1000
MyD88	Cat. # AF5195, Rabbit monoclonal IgG	1:1000
p65	Cat. # AF5006, Rabbit monoclonal IgG	1:1000
p-p65	Cat. # AF2006, Rabbit monoclonal IgG	1:1000
β-Tubulin	Cat. # FD0064, Mouse monoclonal IgG	1:7500

Statistical Analysis

All experiments in this study were repeated at least three times, and the experimental results are expressed as the mean ± standard deviation. Paired comparisons were performed using a *t* test. SPSS software was used to compare the significance of data between groups by one-way ANOVA, and $P < 0.05$ indicated that the data were significant.

Results and Discussion

Isolation and Purification of LCPs-1-A

Crude polysaccharide was extracted from coral powder with a yield of 8.5%. Four components (LCPs-1, LCPs-2, LCPs-3, and LCPs-4) were obtained from DEAE-52 (Fig. 1a). The main component (LCPs-1) was collected and further purified by Sephacryl 300 HR to obtain LCPs-1-A and LCPs-1-B (Fig. 1b). The sugar content of LCPs-1-A was 94.31% by the phenol–sulfuric acid method and the sugar content of LCPs-1-B was low, so the research focused on LCPs-1-A.

Structural Features

According to the UV spectrum (Fig. 1c), LCPs-1-A showed no obvious absorption at 260 nm and 280 nm, suggesting that LCPs-1-A contained almost no nucleic acids or proteins (Zhao et al. 2019).

In the molecular weight chromatogram of LCPs-1-A (Fig. 1d), the retention time of LCPs-1-A was approximately 5.11 min. The molecular weight of LCPs-1-A was 4.90×10^6 Da according to the standard curve of dextran.

FT-IR can be used to analyze the glycosidic bond type, functional group type, and sugar ring configuration of polysaccharides. As shown in Fig. 1e, LCPs-1-A had a strong and wide peak at 3326 cm^{-1}, which was caused by the -OH stretching vibration, which is characteristic of all polysaccharides (Wang et al. 2018b). The absorption peaks at 2900 cm^{-1} and 1412 cm^{-1} were caused by C-H stretching vibrations and bending vibrations, respectively (Han et al. 2021). The band at 1640 cm^{-1} was a water peak, indicating that there was a certain amount of bound water in the polysaccharide (Liu et al. 2019). Bands at 1000–1200 cm^{-1} were caused by the stretching vibrations of C–O–C and C–OH in the pyran structure (Liu et al. 2017a). The signals at 850 cm^{-1} and 578 cm^{-1} were indicative of the α-configuration (Zhang et al. 2016a; Wu et al. 2016). In addition, there was no absorption at 1555 cm^{-1} or 1740 cm^{-1}, suggesting that LCPs-1-A had a low protein content and no uronic acid, respectively (Kpodo et al. 2017; Peng et al. 2019). In summary, the FT-IR results showed that LCPs-1-A had typical structural characteristics of polysaccharides.

According to the monosaccharide composition analysis (Fig. 1f), we knew that LCPs-1-A was mainly composed of glucose. Combined with the FT-IR results, LCPs-1-A might be a glucan composed of α-Glc*p*.

NMR is a powerful method used to analyze polysaccharides, as it can provide some information on the anomeric configuration, glycosidic linkages, repeat units, and so on (Yang et al. 2019). ^1H and ^{13}C NMR experiments of LCPs-1-A were carried out (Fig. 2a, b). LCPs-1-A had two main signal peaks in the anomeric proton region, which were 5.33 ppm and 4.90 ppm; thus, it could be inferred that LCPs-1-A had two sugar residues. The signal at 4.70 ppm came from D_2O, while the protons of C2–C6 between 3.0 and 4.5 ppm were blurred and overlapped, making it difficult to identify the attribution (Yang et al. 2020). In the ^{13}C NMR spectrum, the anomeric carbon signals (99.99 ppm, 98.60 ppm) were the two primary peaks and corresponded to the ^1H-NMR spectrum. However, only one monosaccharide was found to be present by PMP-HPLC analysis, which showed that LCPs-1-A had two connection modes (Wang et al. 2018a). The peaks between 95 and 101 ppm indicated that LCPs-1-A was a polysaccharide with an α configuration (Li et al. 2011). There were no peaks near 82–88 ppm, suggesting the absence of furanose (Zhang et al. 2018). C3 and C5 of pyranose generally appear at shifts below 80 ppm (Li et al. 2020). Therefore, LCPs-1-A contained pyranose but not furanose. The peaks in the range of 60 ~ 90 ppm were attributed to C2 ~ C6 glucose (Li et al. 2020). However, the specific structure of LCPs-1-A cannot be determined due to the presence of various binding sites in polysaccharides.

In summary, LCPs-1-A is highly likely a glucan composed of α-Glc*p* with a molecular weight of 4.90×10^6 Da.

Immunoenhancement Activity of LCPs-1-A

Morphologic Observations and Cell Viability Assay

Morphological changes in RAW264.7 cells can reflect the cell state, and when the cells undergo morphological changes, from round to polygonal morphology, this indicates that the cells are activated (Ueta et al. 2019). According

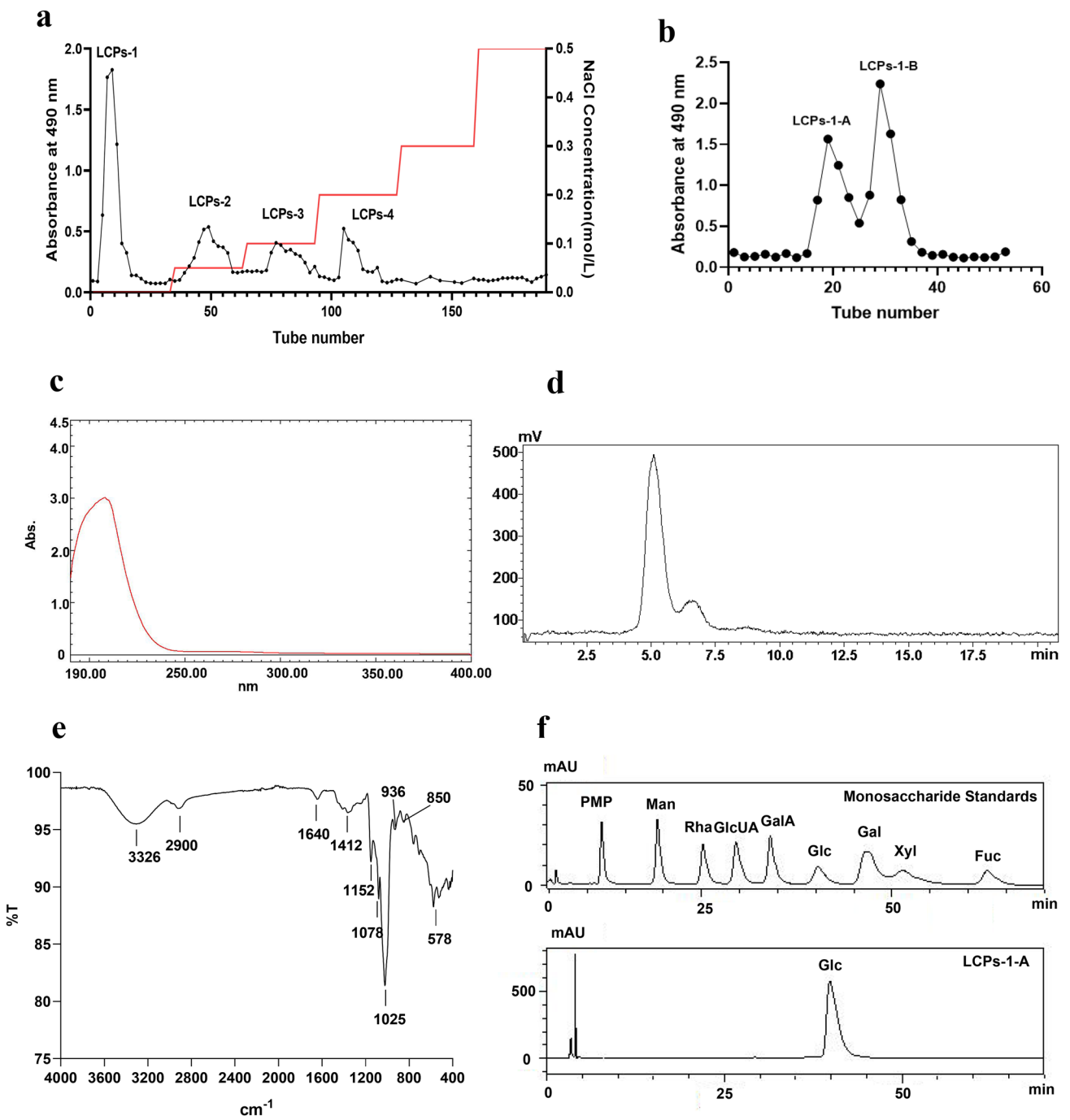

Fig. 1 **a** LCPs was separated by a DEAE-52 column (2.6×30 cm). LCPs-1, LCPs-2, LCPs-3, and LCPs-4 were obtained by eluting with 0, 0.05, 0.1, and 0.2 M NaCl solutions, respectively; **b** the elution curve of LCPs-1 on a Sephacryl 300 HR column; **c** the UV spectrum of LCPs-1-A; **d** the molecule weight by GPC analysis; **e** the FT-IR spectrum of LCPs-1-A; **f** HPLC of monosaccharide composition of LCPs-1-A and monosaccharide standards (Man: mannose, Rha: rhamnose, GlcUA: glucuronic acid, GalA: galacturonic acid, Glc: glucose, Gal: galactose, Xyl: xylose, Fuc: fucose)

to the results (Fig. 3a), the morphology of the cells in the control group showed no change, but the cells in the LCPs-1-A group changed from round to polygonal morphology. These cells were similar to those in the LPS group, indicating that LCPs-1-A had an activating effect. The MTT assay is a simple and classical method to detect the viability and proliferation of cells (Lü et al. 2012). The results (Fig. 3b) showed that LCPs-1-A had no toxic effect on RAW264.7 cells and promoted their proliferation, which was the same tendency as the LPS group.

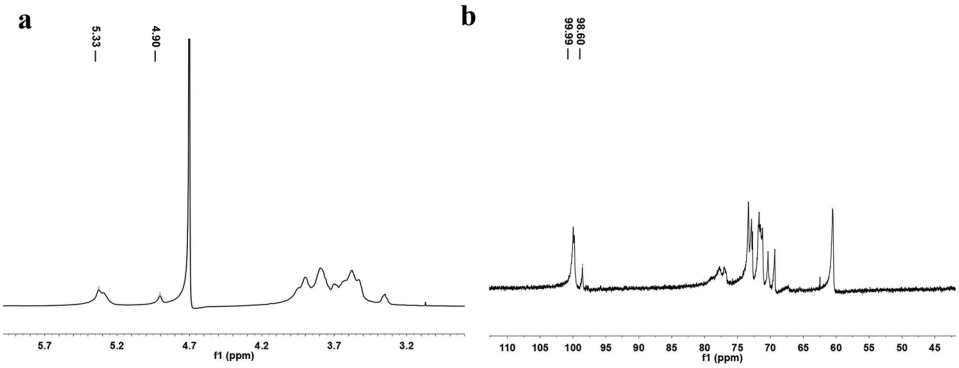

Fig. 2 ^{1}H NMR (**a**) and ^{13}C NMR (**b**) spectra of LCPs-1-A

Neutral Red Uptake Assay and NO Production

Phagocytosis of macrophages is a key indicator to activate cells against pathogens (Liu et al. 2006). After activation, cells will produce NO to prevent the replication of pathogens (Jeong et al. 2019). Therefore, we studied the changes in the phagocytosis and NO production of LCPs-1-A in RAW264.7 cells by a neutral red uptake assay and a NO kit. The results (Fig. 3c, d) showed that with increasing LCPs-1-A concentration, the phagocytic activity of RAW264.7 cells was gradually enhanced, and the release of NO also increased, which was consistent with the trend of the positive drug group.

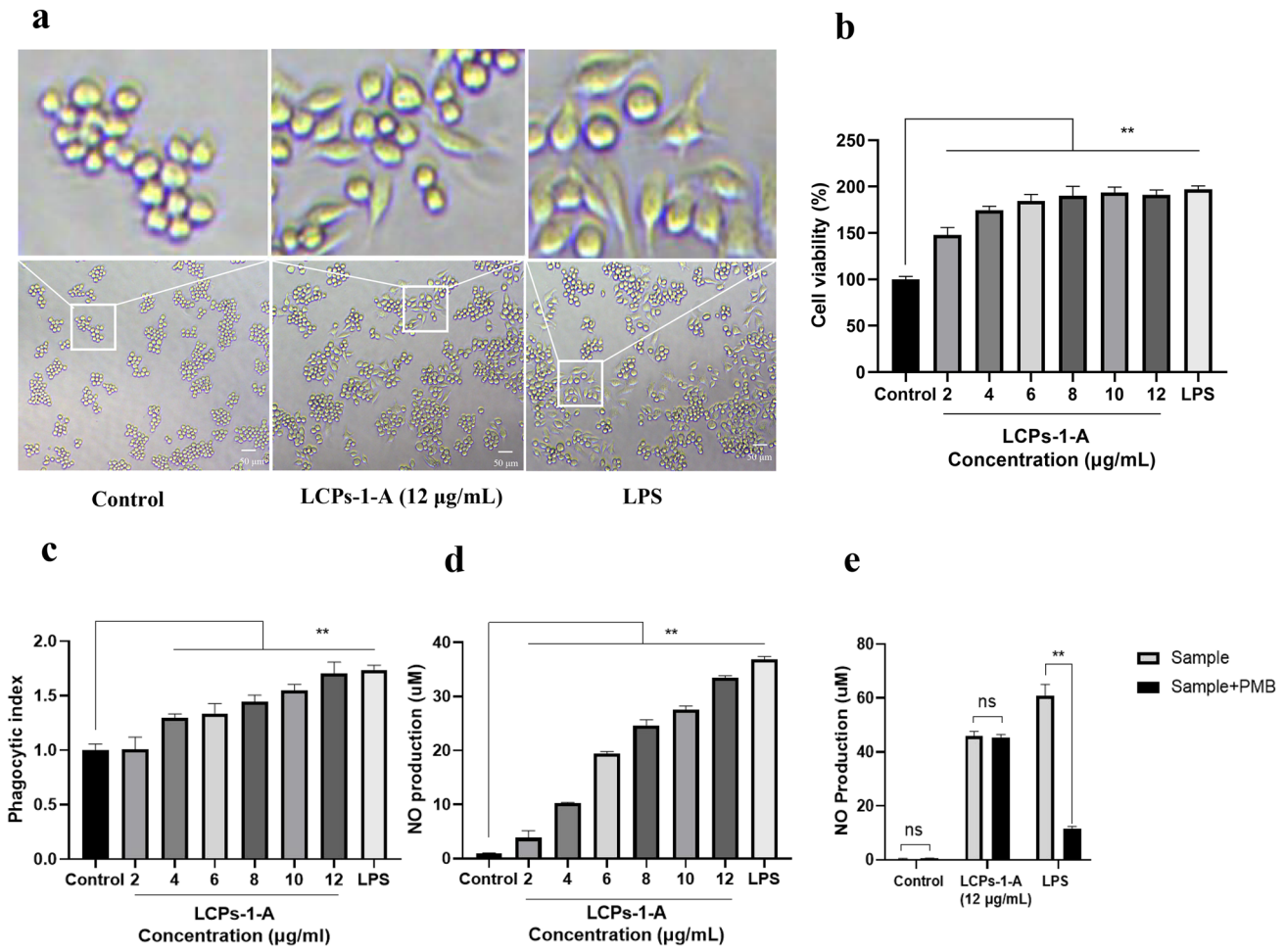

Fig. 3 **a** Morphological changes of cells; **b** effects of LCPs-1-A treatment on the cell viability; **c** effects of the LCPs-1-A on the phagocytosis of RAW264.7 cells; **d** effects of different concentrations of LCPs-1-A on the secretion of NO production; **e** endotoxin contamination tests. Paired comparisons were performed using a *t* test and SPSS software was used for statistical analysis of the data by one-way ANOVA. $*p<0.05$, $**p<0.01$. Values are mean ± SD (standard deviation) ($n=4$). Scale bars: 50 μm

These results suggested that LCPs-1-A could enhance the phagocytosis of cells and produce NO to resist pathogens, thus enhancing immunity. In addition, the interference of endotoxin on LCPs-1-A was excluded in the experiment. As shown in Fig. 3e, the addition of PMB to LCPs-1-A had no effect on NO release from macrophages, indicating that the NO production was caused by LCPs-1-A rather than endotoxin.

Effect of LCPs-1-A on the Production of ROS

ROS at moderate concentrations play an important role in transmitting signals, promoting phagocytosis of cells, and resisting pathogen invasion (Ren et al. 2017). Therefore, ROS are a crucial indicator to evaluate the activation of macrophages. As shown in Fig. 4a, the intensity of the green fluorescence in the LCPs-1-A group (12 μg/mL) was significantly stronger than that of the control group but similar to the LPS group. Figure 4b also showed that ROS secretion in the LCPs-1-A group increased in a dose-dependent manner. These results suggested that LCPs-1-A could promote the secretion of ROS in macrophages, thus enhancing the resistance of cells to pathogens.

Quantitative Real-Time PCR (qRT-PCR) Analysis

The cytokines IL-1β, IL-6, and TNF-α play an indispensable role in immune regulation (Bao et al. 2013). The relationship between LCPs-1-A and IL-1β, IL-6, and TNF-α was verified by qRT-PCR. As shown in Fig. 5a, with increasing LCPs-1-A concentration, the mRNA expression of cytokines IL-1β, IL-6, and TNF-α was notably elevated, which was in agreement with the trend of the LPS group, demonstrating that LCPs-1-A had a good immunoenhancing effect.

Immunofluorescence Assay for NF-κB

NF-κB is an important transcription factor that regulates the expression of genes involved in immune responses in activated macrophages (Han et al. 2018). The most prominent feature of NF-κB activation is the translocation of NF-κB from the cytoplasm into the nucleus. To investigate the effect of LCPs-1-A on NF-κB, an immunofluorescence assay was used. As shown in Fig. 5b, the fluorescence of p65 in the control group indicated that cytoplasmic p65 was not translocated into the nucleus, while the fluorescence marked by red arrows in the LCPs-1-A and LPS groups showed that cytoplasmic p65 had translocated into the nucleus and become activated. Therefore, we concluded that the immunoenhancing activity of LCPs-1-A might be related to the NF-κB signaling pathway.

Western Blot Analysis

Pattern recognition receptors (PRRs) are a class of innate immune system receptors that can recognize and eliminate

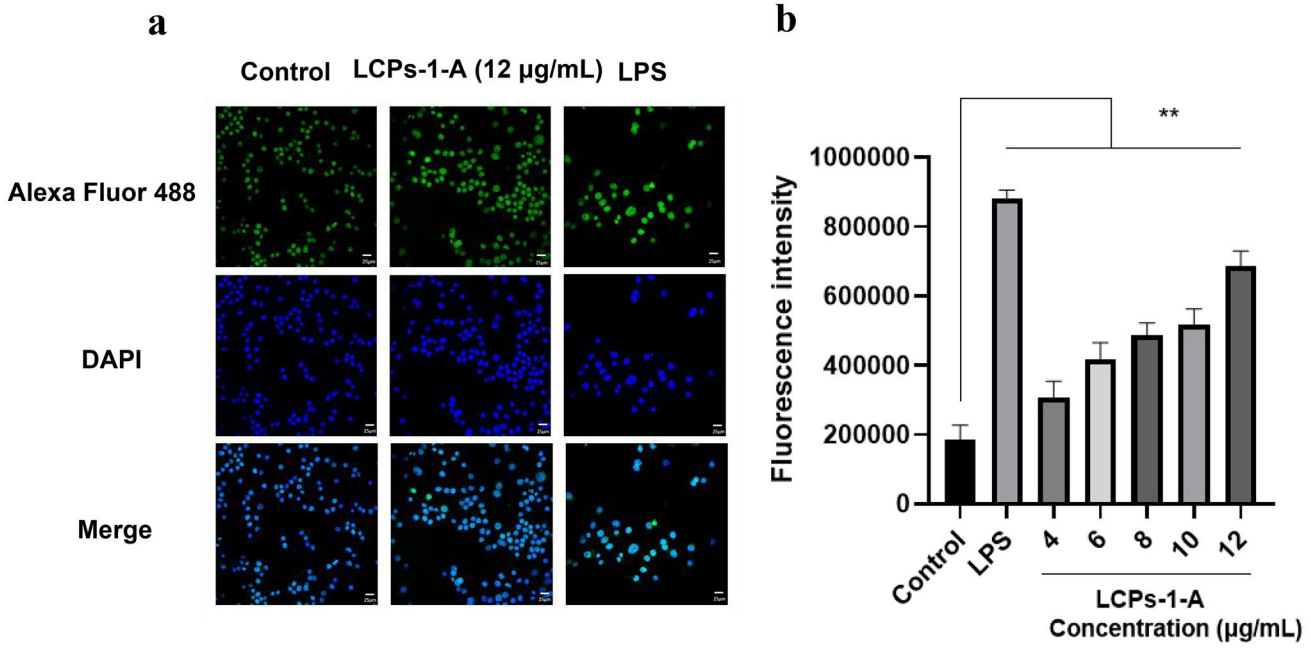

Fig. 4 Fluorescence microscope images (**a**) and quantification (**b**) of ROS secretion in RAW264.7 cells. Paired comparisons were performed using a *t* test and SPSS software was used for statistical analysis of the data by one-way ANOVA. $*p<0.05$, $**p<0.01$ vs. control group. Values are mean ± SD ($n=4$). Scale bars: 25 μm

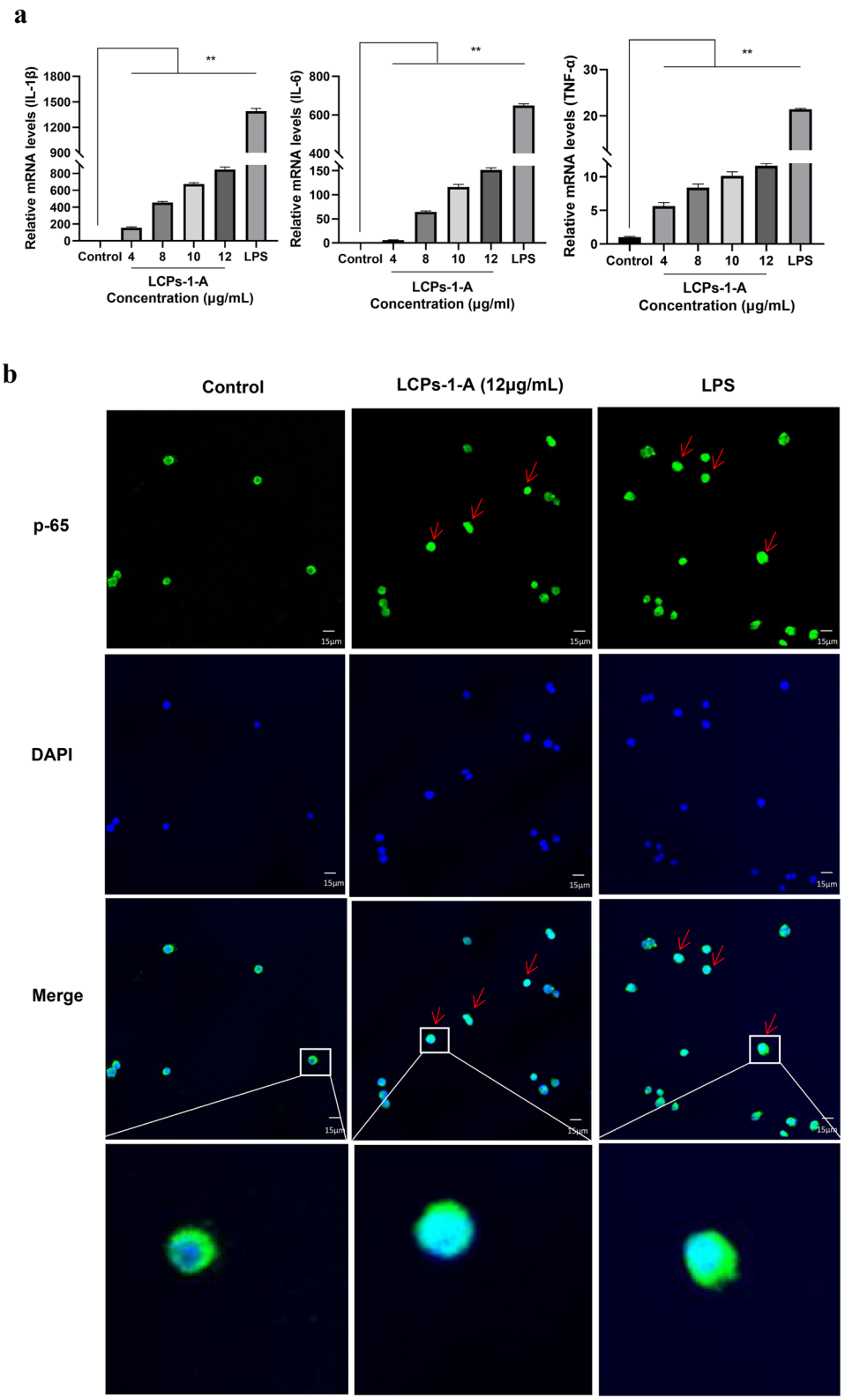

Fig. 5 **a** The effects of LCPs-1-A on the mRNA expression of cytokines (IL-1β, IL-6, and TNF-α) in RAW264.7 cells; **b** nuclear translocation of NF-κB. Paired comparisons were performed using a *t* test and SPSS software was used for statistical analysis of the data by one-way ANOVA. $*p<0.05$, $**p<0.01$ vs. control group. Values are mean ± SD ($n=4$). Scale bars: 15 μm

pathogen invasion (Short et al. 2019). Generally, polysaccharides cannot enter cells directly but are recognized by PRRs on the cytomembrane (Yan et al. 2018) and enter cells mainly through Toll-like receptors (TLRs), complement receptor 3 (CR3), mannose receptor (MR), beta glucan receptor (GR), scavenger receptor I (SR), or Dectin-1 (Wu et al. 2018). As an important class of PRRs, TLRs family has been identified 10 TLRs in humans and 13 TLRs in mice (Kawai and Akira 2006). Among them, TLR4 plays a crucial role in the transmission of many natural polysaccharides

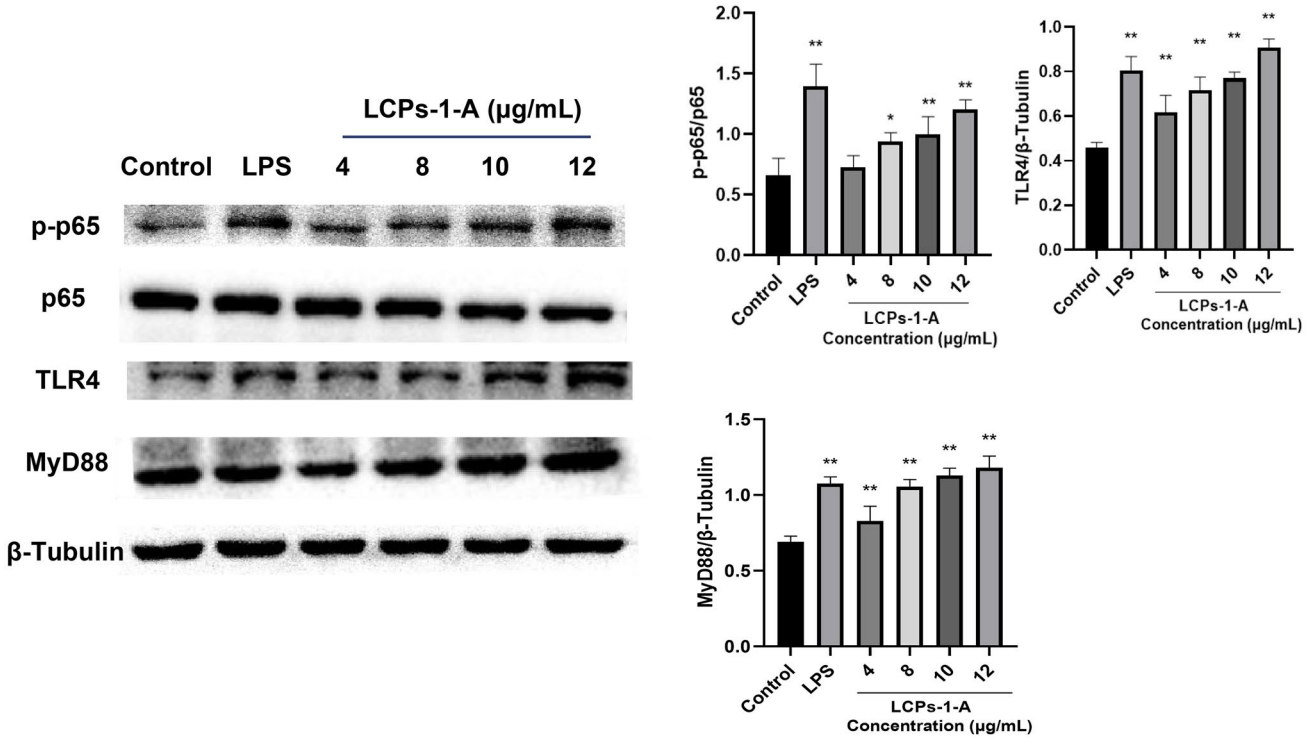

Fig. 6 The expression of p-p65, p-65, TLR4, and MyD88 proteins in RAW264.7 cells. The values of "p-p65/p-65" were calculated by gray-scale value of bands. β-Tubulin was used as total protein loading control. Paired comparisons were performed using a *t* test and SPSS software was used for statistical analysis of the data by one-way ANOVA. $*p<0.05$, $**p<0.01$ vs. control group. Values are mean ± SD ($n=4$)

(Wang et al. 2015; Zhou et al. 2017). Besides, studies have shown that polysaccharides with a major monosaccharide composition consisting of glucose are likely to be TLR4 agonists (Zhang et al. 2016b), and the NF-κB signaling pathway is a classical pathway in immunity (Lawrence 2009). Therefore, we hypothesized that the immunoenhancing effect of LCPs-1-A occurs through the TLR4/NF-κB signaling pathway, and we verified the key proteins p65, p-p65, MyD88 (an adaptor of the TLRs), and TLR4 in this pathway. The results (Fig. 6) showed that different concentrations of

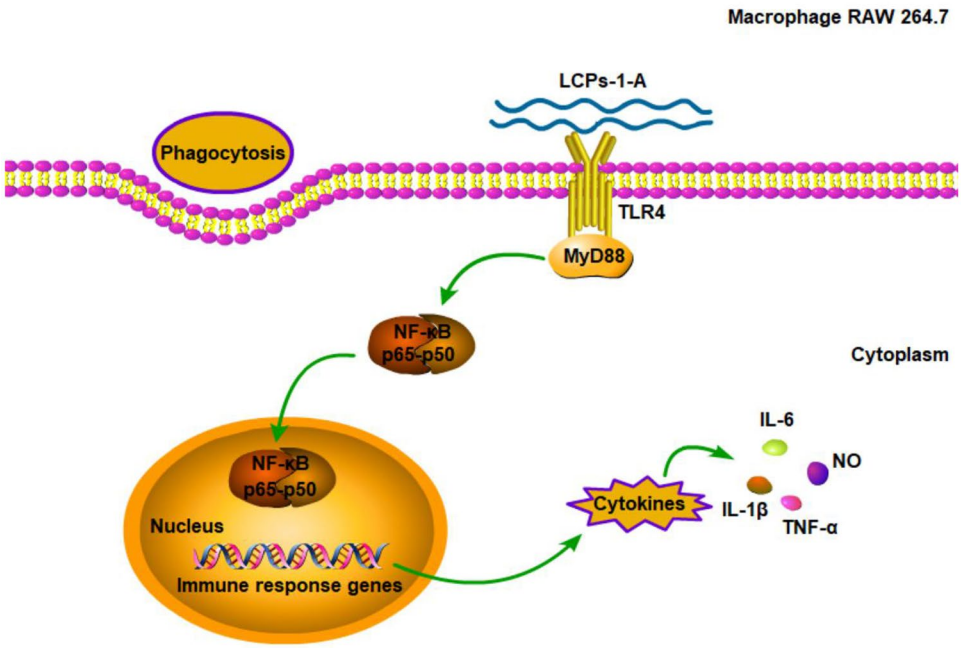

Fig. 7 The possible mechanism of LCPs-1-A-induced macrophages immune enhancement. After LCPs-1-A recognized, TLR4 can recruit MyD88, activate NF-κB, and promote the expression of the proinflammatory cytokines

LCPs-1-A could indeed play an immunoenhancing role similar to LPS. Therefore, we inferred that the immunoenhancing effect of LCPs-1-A might be mediated by the TLR4/NF-κB signaling pathway.

Conclusions

In conclusion, the sugar content of LCPs-1-A obtained from the soft coral *Lobophytum* sp. was 94.31%, and it might be a glucan composed of α-Glc*p* with an average molecular weight of 4.90×10^6 Da. The experiment results indicated that LCPs-1-A is a natural and nontoxic polysaccharide with a good immunoenhancing effect on RAW264.7 cells. Over a range of concentrations, LCPs-1-A promoted the proliferation and phagocytosis of RAW264.7 cells. In addition, it stimulated the secretion of NO and ROS and increased the mRNA expression of related cytokines (IL-1β, IL-6, and TNF-α). The immunoenhancing activity of LCPs-1-A might be due to its effect on the TLR4/NF-κB signaling pathway (Fig. 7). Therefore, LCPs-1-A may be a candidate immune enhancer, which has potential application prospects in medical and food industries.

Author Contribution Xueqin Cao: methodology, data curation, writing (original draft preparation). Qian Zhang: data curation, software, visualization. Yanglu Zhu: visualization, investigation. Siju Li: software. Ying Cai, Pei Li: formal analysis. Deliang Liu, Yun Leng, Simin Ye, Zengmei Xu: writing (review and editing). Hao Li: writing (review and editing), supervision. Lan Liu, Qiongfeng Liao, Baochun Shen: supervision. Zhiyong Xie: project administration.

Funding This work was supported by the National Natural Science Foundation of China (no. U1803123, U1903211, 82074142, 82174104).

Declarations

Competing Interests The authors declare no competing interests.

References

Bao X, Yuan H, Wang C, Liu J, Lan M (2013) Antitumor and immunomodulatory activities of a polysaccharide from *Artemisia argyi*. Carbohydr Polym 98:1236–1243

Chu Q, Zhang S, Yu L, Li Y, Liu Y, Ye X, Zheng X (2019) *Apios americana* Medikus tuber polysaccharide exerts anti-inflammatory effects by activating autophagy. Int J Biol Macromol 130:892–902

Couto D, Zipfel C (2016) Regulation of pattern recognition receptor signalling in plants. Nat Rev Immunol 16:537–552

da Silva BJ, Palhares LCGF, Silva CHF, Sabry DA, Chavante SF, Rocha HAO (2021) In Vitro Antitumor Potential of Sulfated Polysaccharides from Seaweed *Caulerpa cupressoides* var. *flabellata*. Mar Biotechnol 23:77–89

Dubois M, Gilles KA, Hamilton JK, Rebers PT, Smith F (1956) Colorimetric Method for Determination of Sugars and Related Substances. Anal Chem 28:350–356

Gao X, Meng X, Li J, Tong H (2009) Isolation, Characterization and Hypoglycemic Activity of an Acid Polysaccharide Isolated from *Schisandra chinensis* (Turcz.) Baill. Lett Org Chem 6:428–433

Han L, Yu J, Chen Y, Cheng D, Wang X, Wang C (2018) Immunomodulatory Activity of Docosahexenoic Acid on RAW264.7 Cells Activation through GPR120-Mediated Signaling Pathway. J Agric Food Chem 66:926–934

Han Y, Wu Y, Li G, Li M, Yan R, Xu Z, Lei H, Sun Y, Duan X, Hu L, Huang R (2021) Structural characterization and transcript-metabolite correlation network of immunostimulatory effects of sulfated polysaccharides from green alga *Ulva pertusa*. Food Chem 342:128537

Jeong M, Kim JH, Yang H, Kang SD, Song S, Lee D, Lee JS, Yoon Park JH, Byun S, Lee KW (2019) Heat-Killed *lactobacillus plantarum* KCTC 13314BP enhances phagocytic activity and immunomodulatory effects via activation of MAPK and STAT3 pathways. J Microbiol Biotechnol 29:1248–1254

Kawai T, Akira S (2006) TLR signaling. Cell Death Differ 13:816–825

Kpodo FM, Agbenorhevi JK, Alba K, Bingham RJ, Oduro IN, Morris GA, Kontogiorgos V (2017) Pectin isolation and characterization from six okra genotypes. Food Hydrocoll 72:323–330

Lawrence T (2009) The nuclear factor NF-kappaB pathway in inflammation. Cold Spring Harb Perspect Biol 1:a001651

Lee KS, Shin JS, Nam KS (2011) Cancer chemopreventive effects of starfish polysaccharide in human breast cancer cells. Biotechnol Bioprocess Eng 16:987–991

Li H, Mi Y, Duan Z, Ma P, Fan D (2020) Structural characterization and immunomodulatory activity of a polysaccharide from *Eurotium cristatum*. Int J Biol Macromol 162:609–617

Li J, Fan L, Ding S (2011) Isolation, purification and structure of a new water-soluble polysaccharide from *Zizyphus jujuba cv Jinsixiaozao*. Carbohydr Polym 83:477–482

Liao J, Li C, Huang J, Liu W, Chen H, Liao S, Chen H, Rui W (2018) Structure characterization of honey-processed *astragalus* polysaccharides and its anti-inflammatory activity in vitro. Molecules 23:168

Lin S, Li HY, Yuan Q, Nie XR, Zhou J, Wei SY, Du G, Zhao L, Wang SP, Zhang Q, Chen H, Qin W, Wu DT (2020) Structural characterization, antioxidant activity, and immunomodulatory activity of non-starch polysaccharides from *Chuanminshen violaceum* collected from different regions. Int J Biol Macromol 143:902–912

Liu C, Leung MY, Koon JC, Zhu LF, Hui YZ, Yu B, Fung KP (2006) Macrophage activation by polysaccharide biological response modifier isolated from *Aloe vera* L. var. *chinensis* (Haw.) Berg. Int Immunopharmacol 6:1634–1641

Liu D, Sun Q, Xu J, Li N, Lin J, Chen S, Li F (2017a) Purification, characterization, and bioactivities of a polysaccharide from mycelial fermentation of *Bjerkandera fumosa*. Carbohydr Polym 167:115–122

Liu GK, Li N, Song SY, Zhang YJ, Wang JR (2019) Three exopolysaccharides from the liquid fermentation of *Polyporus umbellatus* and their bioactivities. Int J Biol Macromol 132:629–640

Liu W, Wang H, Yu J, Liu Y, Lu W, Chai Y, Liu C, Pan C, Yao W, Gao X (2016) Structure, chain conformation, and immunomodulatory activity of the polysaccharide purified from Bacillus Calmette Guerin formulation. Carbohydr Polym 150:149–158

Liu X, Sun Z, Zhang M, Meng X, Xia X, Yuan W, Xue F, Liu C (2012) Antioxidant and antihyperlipidemic activities of polysaccharides from sea cucumber *Apostichopus japonicus*. Carbohydr Polym 90:1664–1670

Liu X, Xie J, Jia S, Huang L, Wang Z, Li C, Xie M (2017b) Immunomodulatory effects of an acetylated *Cyclocarya paliurus*

polysaccharide on murine macrophages RAW264.7. Int J Biol Macromol 98:576–581
Lü L, Zhang L, Wai MS, Yew DT, Xu J (2012) Exocytosis of MTT formazan could exacerbate cell injury. Toxicol Vitr 26:636–644
Molinski TF, Dalisay DS, Lievens SL, Saludes JP (2009) Drug development from marine natural products. Nat Rev Drug Discov 8:69–85
Mosmann T (1983) Rapid Colorimetric Assay for Cellular Growth and Survival: Application to Proliferation and Cytotoxicity Assays. J Immunol Methods 65:55–63
Peng B, Luo Y, Hu X, Song L, Yang J, Zhu J, Wen Y, Yu R (2019) Isolation, structural characterization, and immunostimulatory activity of a new water-soluble polysaccharide and its sulfated derivative from *Citrus medica* L. var. *sarcodactylis*. Int J Biol Macromol 123:500–511
Rastogi RP, Singh SP, Häder DP, Sinha RP (2010) Detection of reactive oxygen species (ROS) by the oxidant-sensing probe 2',7'-dichlorodihydrofluorescein diacetate in the cyanobacterium *Anabaena variabilis* PCC 7937. Biochem Biophys Res Commun 397:603–607
Ren Y, Zheng G, You L, Wen L, Li C, Fu X, Zhou L (2017) Structural characterization and macrophage immunomodulatory activity of a polysaccharide isolated from *Gracilaria lemaneiformis*. J Funct Foods 33:286–296
Ruocco N, Costantini S, Guariniello S, Costantini M (2016) Polysaccharides from the marine environment with pharmacological, cosmeceutical and nutraceutical potential. Molecules 21:551
Sadhu A, Moriyasu Y, Acharya K, Bandyopadhyay M (2019) Nitric oxide and ROS mediate autophagy and regulate *Alternaria alternata* toxin-induced cell death in tobacco BY-2 cells. Sci Rep 9:1–14
Safari E, Hassan ZM (2020) Immunomodulatory effects of shark cartilage: Stimulatory or anti-inflammatory. Process Biochem 92:417–425
Schepetkin IA, Quinn MT (2006) Botanical polysaccharides: Macrophage immunomodulation and therapeutic potential. Int Immunopharmacol 6:317–333
Shen H, Liu X, Jiang M, Luo G, Wu Z, Chen B, Li J, Liu L, Chen S (2019) Anti-inflammatory cembrane-type diterpenoids and prostaglandins from soft coral *lobophytum sarcophytoides*. Mar Drugs 17:481
Short KK, Miller SM, Walsh L, Cybulski V, Bazin H, Evans JT, Burkhart D (2019) Co-encapsulation of synthetic lipidated TLR4 and TLR7/8 agonists in the liposomal bilayer results in a rapid, synergistic enhancement of vaccine-mediated humoral immunity. J Control Release 315:186–196
Simmons TL, Andrianasolo E, McPhail K, Flatt P, Gerwick WH (2005) Marine natural products as anticancer drugs. Mol Cancer Ther 4:333–342
Song X, Ren T, Zheng Z, Lu T, Wang Z, Du F, Tong H (2017) Antitumor and immunomodulatory activities induced by an alkali-extracted polysaccharide BCAP-1 from *Bupleurum chinense via* NF-κB signaling pathway. Int J Biol Macromol 95:357–362
Synytsya A, Choi DJ, Pohl R, Na YS, Capek P, Lattová E, Taubner T, Choi JW, Lee CW, Park JK, Kim WJ, Kim SM, Lee J, Park YI (2015) Structural Features and Anti-coagulant Activity of the Sulphated Polysaccharide SPS-CF from a Green Alga *Capsosiphon fulvescens*. Mar Biotechnol 17:718–735
Takeuchi O, Akira S (2010) Pattern Recognition Receptors and Inflammation. Cell 140:805–820
Ueta M, Takaoka K, Yamamura M, Maeda H, Tamaoka J, Nakano Y, Noguchi K, Kishimoto H (2019) Effects of TGF-β1 on the migration and morphology of RAW264.7 cells in vitro. Mol Med Rep 20:4331–4339
Velkov T, Roberts KD, Nation RL, Thompson PE, Li J (2013) Pharmacology of polymyxins: new insights into an "old" class of antibiotics. Future Microbiol 8:711–724
Wang L, Chen L, Li J, Di L, Wu H (2018a) Structural elucidation and immune-enhancing activity of peculiar polysaccharides fractioned from marine clam *Meretrix meretrix* (Linnaeus). Carbohydr Polym 201:500–513
Wang M, Yang XB, Zhao JW, Lu CJ, Zhu W (2017) Structural characterization and macrophage immunomodulatory activity of a novel polysaccharide from *Smilax glabra Roxb*. Carbohydr Polym 156:390–402
Wang M, Zhao S, Zhu P, Nie C, Ma S, Wang N, Du X, Zhou Y (2018b) Purification, characterization and immunomodulatory activity of water extractable polysaccharides from the swollen culms of *Zizania latifolia*. Int J Biol Macromol 107:882–890
Wang Y, Lai L, Teng L, Li Y, Cheng J, Chen J, Deng C (2019) Mechanism of the anti-inflammatory activity by a polysaccharide from *Dictyophora indusiata* in lipopolysaccharide-stimulated macrophages. Int J Biol Macromol 126:1158–1166
Wang Z, Dong B, Feng Z, Yu S, Bao Y (2015) A study on immunomodulatory mechanism of Polysaccharopeptide mediated by TLR4 signaling pathway. BMC Immunol 16:1–9
Weeks BA, Keisler AS, Myrvik QN, Warinner JE (1987) Differential uptake of neutral red by macrophages from three species of estuarine fish. Dev Comp Immunol 11:117–124
Wu F, Zhou C, Zhou D, Ou S, Zhang X, Huang H (2018) Structure characterization of a novel polysaccharide from: *Hericium erinaceus* fruiting bodies and its immunomodulatory activities. In: Food Funct 9:294–306
Wu M, Feng H, Song J, Chen L, Xu Z, Xia W, Zhang W (2020) Structural elucidation and immunomodulatory activity of a neutral polysaccharide from the Kushui Rose (*Rosa setate x Rosa rugosa*) waste. Carbohydr Polym 232:115804
Wu Y, Li Y, Liu C, Li E, Gao Z, Liu C, Gu W, Huang Y, Liu J, Wang D, Hu Y (2016) Structural characterization of an acidic Epimedium polysaccharide and its immune-enhancement activity. Carbohydr Polym 138:134–142
Yan J, Han Z, Qu Y, Yao C, Shen D, Tai G, Cheng H, Zhou Y (2018) Structure elucidation and immunomodulatory activity of a β-glucan derived from the fruiting bodies of *Amillariella mellea*. Food Chem 240:534–543
Yang D, Lin F, Huang Y, Ye J, Xiao M (2020) Separation, purification, structural analysis and immune-enhancing activity of sulfated polysaccharide isolated from sea cucumber viscera. Int J Biol Macromol 155:1003–1018
Yang J, Tu J, Liu H, Wen L, Jiang Y, Yang B (2019) Identification of an immunostimulatory polysaccharide in banana. Food Chem 277:46–53
Ye F, Zhou YB, Li J, Gu YC, Guo YW, Li XW (2020) New steroids from the South China sea soft coral *Lobophytum sp*. Chem Biodivers 17:e2000214
Younes I, Rinaudo M (2015) Chitin and chitosan preparation from marine sources. Structure, properties and applications. Mar Drugs 13:1133–1174
Yu Q, Nie SP, Li WJ, Zheng WY, Yin PF, Gong DM, Xie MY (2013) Macrophage immunomodulatory activity of a purified polysaccharide isolated from *Ganoderma atrum*. Phyther Res 27:186–191
Yuan L, Zhong ZC, Liu Y (2020) Structural characterisation and immunomodulatory activity of a neutral polysaccharide from *Sambucus adnata* Wall. Int J Biol Macromol 154:1400–1407
Zhang M, Wang G, Lai F, Wu H (2016a) Structural Characterization and Immunomodulatory Activity of a Novel Polysaccharide from *Lepidium meyenii*. J Agric Food Chem 64:1921–1931
Zhang X, Qi C, Guo Y, Zhou W, Zhang Y (2016b) Toll-like receptor 4-related immunostimulatory polysaccharides: Primary structure, activity relationships, and possible interaction models. Carbohydr Polym 149:186–206
Zhang Y, Zeng Y, Men Y, Zhang J, Liu H, Sun Y (2018) Structural characterization and immunomodulatory activity of exopolysaccharides from submerged culture of *Auricularia auricula-judae*. Int J Biol Macromol 115:978–984

Zhao Y, Hu W, Zhang H, Ding C, Huang Y, Liao J, Zhang Z, Yuan S, Chen Y, Yuan M (2019) Antioxidant and immunomodulatory activities of polysaccharides from the rhizome of *Dryopteris crassirhizoma* Nakai. Int J Biol Macromol 130:238–244

Zhou L, Liu Z, Wang Z, Yu S, Long T, Zhou X, Bao Y (2017) *Astragalus* polysaccharides exerts immunomodulatory effects *via* TLR4-mediated MyD88-dependent signaling pathway *in vitro* and *in vivo*. Sci Rep 7:1–13

Zhu Q, Lin L, Zhao M (2020) Sulfated fucan/fucosylated chondroitin sulfate-dominated polysaccharide fraction from low-edible-value sea cucumber ameliorates type 2 diabetes in rats: New prospects for sea cucumber polysaccharide based-hypoglycemic functional food. Int J Biol Macromol 159:34–45